Ultra-low temperature reactive spark plasma sintering of ZrB_2-hBN ceramics

Zou, Ji; Zhang, Guo Jun; Shen, Zhi Jian; Binner, JGP

DOI:
10.1016/j.jeurceramsoc.2016.01.044

Document Version
Peer reviewed version

Citation for published version (Harvard):
Zou, J, Zhang, GJ, Shen, ZJ & Binner, JGP 2016, 'Ultra-low temperature reactive spark plasma sintering of ZrB_2-hBN ceramics', *Journal of the European Ceramic Society*, vol. 36, no. 15, pp. 3637-3645. https://doi.org/10.1016/j.jeurceramsoc.2016.01.044

Ultra-Low Temperature Reactive Spark Plasma Sintering of ZrB_2- *h*BN ceramics

Ji Zou[a*], Guo-Jun Zhang[b], Zhi-Jian Shen[c,d] and Jon Binner[a]

[a] *School of Metallurgy and Materials, University of Birmingham, B15 2TT, Birmingham, UK.*

[b] *State Key Laboratory for Modification of Chemical Fibers and Polymer Materials, Donghua University, Shanghai 201620, China*

[c] *School of Materials Science and Engineering, Tsinghua University, 100084, Beijing, China*

[d] *Department of Materials and Environmental Chemistry, Arrhenius Laboratory, Stockholm University, S-106 91 Stockholm, Sweden.*

Abstract

Starting from ZrN and amorphous boron, dense ZrB_2 ceramics with 37vol% hexagonal BN were consolidated by spark plasma sintering. Benefiting from the moderate exothermic reaction between ZrN and B and the resultant fine powder generated, ZrB_2-BN ceramics with relative density of 94% could be reached at 1100^{o}C, further improved to 97% by 1550^{o}C. The effects of sintering temperature and holding time on the densification behavior, microstructural evolution and mechanical properties of ZrB_2-BN ceramics were investigated. ZrB_2-37vol%BN ceramics densified at 1700^{o}C exhibited attractive mechanical performance: a three-point bending strength of 353MPa, a Vicker's hardness of 6.7 GPa and a Young's modulus of 197.5 GPa. Note that its strength dropped sharply to 191MPa measured at 1300^{o}C. The combination of low sintering temperature (1100-1550^{o}C), low Young's modulus (180-200GPa) and relatively high strength (200-350MPa) make reactively sintered ZrB_2-BN composites as promising matrix for continuous fiber reinforced composites.

*Corresponding author

Ji Zou, email: j.zou@bham.ac.uk; zouji1983@aliyun.com

Tel: +44-(0)7478454102; Fax: +44 (0)121 414 3971

Keywords: Reactive sintering; Spark plasma sintering; Ultra-high temperature ceramics; Mechanical property; Hexagonal boron nitride.

1. Introduction

The future advanced design of hypersonic vehicles might enable flights in the near-earth atmosphere to operate at speeds over Mach 5, this would mean that a rapid transport around the earth in 2-3 hours would become reality if all the significant technical issues could be solved. One of the challenges that needs to be overcome is the development of materials that can survive the extreme conditions, which will be faced by the thermal protection system and propulsion components. The sharp leading edges and nose cones of hypersonic aerospace vehicles are expected to be exposed an environment consisting of a low partial pressure of molecular and dissociated oxygen, high heat fluxes (>1 MW/m^2, depending on the geometry), severe ablation and very high temperatures (>2000^oC) when the velocity exceeds Mach 7 [1-3].

Benefiting from a combination of high melting point (>3000^oC), superior structural stability at elevated temperatures, excellent mechanical properties, in terms of stiffness, strength and hardness, and high thermal conductivity, refractory metal diborides and carbides, such as ZrB_2, HfB_2, ZrC and HfC are being considered as the potential candidates for aforementioned applications. Known as Ultra-high Temperature Ceramics, UHTCs [2-3], these materials lack toughness and thermal shock resistance however; monolithic UHTCs are susceptible to undergo catastrophic failure when exposed to mechanical shocks in such extreme environments [2]. Although the intrinsic brittleness could be modified and improved in UHTCs through a careful microstructure design [4], reinforcing UHTCs matrices by continuous carbon or SiC fibers has been shown to have greater potential [5].

Processing these materials is not easy, however, owing to their strong covalent bonding; sintering temperatures over 1800^oC and high pressures over 30 MPa are routinely needed to achieve full densification in UHTCs, even with the use of sintering additives [2]. Unfortunately, commercial Nicalon^{TM} (Nippon Carbon, Japan) SiC fibers, which have relatively high oxygen content, typically about 12 wt%, cannot withstand such high sintering temperature due to the decomposition of the Si-O-C phase and the deformation of fibers under pressure. Whilst low crystallinity Hi-Nicalon^{TM} SiC fiber with much lower oxygen levels (<0.5 wt %) have been demonstrated to have a better structural stability [6], their degradation in a ZrB_2-$ZrSi_2$ matrix occurred at only 1600^oC. Only 26% of the

fibers maintained their pristine aspect [7]. Similar, though less pronounced, degradation was even observed in the third generation Tyranno^{TM} SiC fiber [8] reinforced ZrB_2-$ZrSi_2$ composites at the same temperature [7].

Continuous fiber/UHTC composite (CF/UHTC) have been prepared by alternative approaches involving much lower fabrication temperature, e.g. <1400^{o}C. These include chemical vapor infiltration (CVI) [9], polymer impregnation and pyrolysis (PIP) [10], slurry vacuum infiltration (SVI) [11] and reaction melt-infiltration (RMI) [12]. Among these approaches, only RMI could achieve a final composite with a relative density higher than 95% [12]. Unfortunately, below 1400^{o}C, the infiltrated phase is limited to silicon due to its melting temperature. Residual silicon is very difficult to remove after RMI, which can impair the high temperature mechanical properties of the final composites.

In order to reduce the residual porosity in CF/UHTC, a further step, e.g. involving hot pressing to densify the matrix and reduce the gap between fiber and matrix is necessary [13-14]. Considering the state-of-the-art SiC fibers available in the market, the desired post processing temperature must be lower than about 1600^{o}C, ideally, lower than about 1500^{o}C. If this could be achieved, the integrity and mechanical performance of the fibers could be retained. Numerous additives have been investigated with respect to decreasing the densification temperature of UHTCs. Taking ZrB_2-based ceramics as an example, carbides, nitrides, silicates and a variety of metals have all been added. For instance, B_4C and WC could react and remove the oxygen contamination on the surface of ZrB_2 powders, thereby increasing the driving force for densification [15]. To date, however, dense ZrB_2-based composites have only been obtained using densification temperatures above 1800^{o}C since the sintering activated by the presence of the carbide was actually realized via a solid state approach through enhanced grain boundary diffusion in the ZrB_2. Disilicides, in the form of $MoSi_2$, $TaSi_2$ and $ZrSi_2$ [16-17], have also been added into ZrB_2 ceramics. As a result of the generation of intergranular low-temperature eutectics with ZrB_2, the minimum densification temperature for this system could be reduced from 1800^{o}C for ZrB_2-$MoSi_2$ to 1550^{o}C for ZrB_2-$ZrSi_2$ ceramics during hot pressing [17]. As a result, 10 vol% $ZrSi_2$ additives were used to fabricate SiC_f/ZrB_2 composites by several research groups; nevertheless, the reaction between the $ZrSi_2$ and SiC fibers could not be ignored during processing [5, 7]. In addition, the softening of the $ZrSi_2$ phase above 1400^{o}C limited their high temperature performance.

Recently, the fine ZrB_2 powder coated with a BN shell had been successfully synthesized in our group between 1100-1300°C [18]. The fine BN@ZrB_2 core shell had a narrow particle size distribution, which suggests it would have superior sinterability. In this paper, detailed work on the direct reactive sintering of ZrB_2-*h*BN composites from ZrN and B will be presented. The aim was to densify the composite at as low a temperature as possible, then investigate its mechanical performance and to explore its potential application as a matrix for long SiC fiber reinforced composites.

2. Experimental procedure

ZrN (>99.8% purity, average particle size 10 µm, grade ZR-301, Atlantic Equipment Engineers, Bergenfield, NJ, USA) and amorphous boron (>96.5% purity, Mg: 0.8wt%, specific surface area >10 m^2/g, H.C. Starck, Germany) powders were mixed in a polyethylene bottle for 24 h using ethanol as the liquid and 3 mol% yttria partially stabilised zirconia, 3Y-PSZ, balls with a diameter of 10 mm as the mixing media. According to reaction 1 below, the molar ratio between ZrN and B needed to be set at 3: 1, however, since the boron powder was not pure and the impurities consisted of some volatile phases, the final composition included an excess of 3 wt% boron compared with the stoichiometric ratio.

$$ZrN + 3B \rightarrow ZrB_2 + BN \text{ (Reaction 1)}$$

For some batches, 10 wt% β-SiC whiskers were added into the ZrN - B mixtures, whilst the process route remained the same.

Rotary evaporation at 70°C under a vacuum of 10.1 kPa was used to dry the milled powder out of the slurry and the resulting powder cakes were crushed using a mortar and pestle made of high purity Al_2O_3. The powders were then loaded into a graphite die lined with graphite foil and the die surrounded with two layers of porous carbon felt insulation with the goal of achieving a more homogeneous temperature distribution across the powder during sintering. The latter was undertaken using spark plasma sintering (SPS, Type HP D 25/1, FCT System, Rauenstein, Germany) under a vacuum of ~5 Pa. During sintering, the samples were heated at 100°C/min to a series of temperatures in the range 1100 to 2000°C and two holding times of 7 and 20 mins were used. Above 400°C, the temperature was monitored by an infrared pyrometer placed vertically above the sample and focused near its

center [19]. At first, a minimum pressure of ~4MPa was kept on the sample during heating to provide a current path. The pressure was gradually increased to 60MPa over a period of few seconds at the onset of the holding time and it was removed when sintering was completed. Two typical sintering profiles are illustrated in Figure 1.

The surfaces of each of the densified pellet were ground to a 120 grit finish for removing all the carbon contaminated layers. Subsequently, the bulk densities and open porosity of as-sintered samples were determined by the Archimedes method. X-ray diffractometry (XRD, Seifert, Ahrensburg, Germany) was used to determine the phase assemblage on the polished ceramics, it changed of 0.01° with a step of 1 s. A theoretical value of 4.67 g/cm^3 was used to estimate the relative sintered density of the ZrB_2-37 vol% *h*BN composites (known as ZBN) based on the law of mixtures. Individual values of 6.09 g/cm^3 for the ZrB_2 and 2.27 g/cm^3 for the hBN were used for the calculation, according to the JCPDF cards 34-0432 and 34-0421.

The microstructures of the ZBN composites were examined by scanning electron microscopy (SEM; XL30-FEG, FEI, Eindhoven, Netherlands). Unless otherwise specified, the specimens were each polished using progressively finer diamond abrasives down to a 1 µm particle size. Given the residual porosity in the samples sintered at below 1550^{o}C, a Focused Ga^+ Ion Beam (FIB, Quanta 3D FEG, FEI, Eindhoven, Netherlands) was employed to polish these samples through a mode of cleaning cross section [20]. During FIB cutting, the ion beam current was gradually decreased from 65 to 0.1 nA until a flat, polished surface with dimensions of about 20 × 20 µm was achieved. For transmission electron microscopy (TEM, 200 kV, JEOL 2100F, Japan) observation, 3 mm diameter discs were cut from sintered pellets and these were reduced in thickness to about 100 µm foils using mechanical polishing. They were finally thinned by argon ion beam milling at 5 kV until perforations could be observed by optical microscopy.

In terms of mechanical property characterization, the Vickers hardness, HV_1, was measured (Model FV-700, Future-Tech Corp., Tokyo, Japan) on the polished surface of sintered ceramics with an indentation load of 9.81 N. The elastic modulus (E), shear modulus (G) and Poisson's ratio (v) were all measured by an impulse excitation technique (IET, Grindo-Sonic, Lemmens N.V., Leuven, Belgium). For IET measurement, the resonance frequency was

collected from sample discs with a diameter of ~30mm and a thickness of ~3mm. Three-point bending strength was measured on the rectangular bars (25 mm × 2.5 mm × 2 mm) at room temperature in air and 1300°C in flowing argon, respectively. A crosshead displacement of 0.5 mm/min was used during strength measurements.

3. Results and discussion

3.1 Densification behaviour

The sintering profiles of ZBN ceramics densified at 1100 and 1500°C are shown in Fig.1a and b, respectively. Samples sintered at other temperatures showed similar features as appeared in Fig.1 and their curves are therefore not displayed here. It will be observed that whilst the temperature was being raised, the displacement of the SPS punch displayed a linear expansion. Such a linear relationship indicates that no significant densification occurred during this heating period, either from particle arrangement or formation of particle necks. The movement of the punch originated from thermal expansion of the system. The presence of significant densification in the samples would result in a deviation from linearity in the punch displacement such as may be observed in Fig. 1b after approximately 18 mins.

The pressure during sintering was always applied when temperature reached the selected value, so, for Fig.1a this was 1100°C. It will be observed that about 20 seconds later, there was a sudden increase in temperature combined with substantial shrinkage in the sample. Such a heat release supports the idea that the ZrN reacted with the boron at this moment. Thermodynamically, reaction 1 is favorable at room temperature ($\Delta G^{o}_{rxn} = -206\ kJ$ at 300 K), and the Gibbs energy becomes more negative as the temperature increases. The reaction has been confirmed as a self-propagating high temperature synthesis, SHS, process in our previous work [18]. Since the temperature peak occurred after application of the pressure, the precursor particles will have been packed closer in the current work, allowing reaction 1 to be initiated more easily. However, at only 1100°C no further evidence of densification was observed, even with the longer holding time. Density measurements, Fig. 2, also verified that the effect of the holding time on the final density of the ZBN composite was fairly insignificant at low sintering temperatures. For example, at 1100°C the relative density

increased from just below 92% to ~94% when the holding time was changed from 7 to 20 min. Just over half of the porosity was open after 7 mins of holding time (~4.2% of ~8%), with this decreasing to just under half, ~2.5% of ~6%, after 20 mins.

A similar exothermic peak at just above 1100^{o}C was also observed in the temperature profile for the ZBN composite densified at 1550^{o}C, Fig. 1b. However, since the pressure of 60MPa was only applied when the desired sintering temperature was reached, the degree of shrinkage between the onset of the reaction and the application of the pressure was minimal. Therefore, the sample was still in a highly porous status after reaction, if no high pressure was applied. The densification and reaction periods were separated in Fig.1b, because a more evident shrinkage appeared at 1550^{o}C under 60MPa. The final density of the ZBN composite increased from 94% after being sintered for 20 mins at 1100^{o}C to 97% when 1550^{o}C was used and consequently most of the porosity became closed, only ~1.5% remained open. A further increase in the density of the ZBN composites could be realized either by extending the holding time or by increasing the sintering temperature, as illustrated in Figure 2. As expected, elevating the sintering temperature was more effective, though the difference between 7 and 20 mins of holding time gradually decreased to zero by the sintering temperature of 2000^{o}C.

3.2 Phase and microstructure evolution

Figures 3 and 4 show the microstructure evolution of the ZBN composites as a function of sintering temperature. In a separate experiment, for one sample after the appearance of the exothermic peak, see Figure 1a, the furnace was immediately turned off. Subsequent SEM analysis confirmed that the result was agglomerates ~2 μm in diameter that were composed of crystallites with an average size of ~200 nm (Figure 3a). XRD analysis revealed that the powder, labelled 'SHS' in Figure 5a, was constituted by a mixture of crystalline *h*BN and ZrB_2. Note that an extra peak at a 2θ value of ~27^{o} was also detected; it is currently unknown what this represents but it was very small in the as-synthesised powder. Comparing the XRD data collected from the polished surfaces of the sintered ZBN composite sintered at 1100^{o}C with that from the SHS powder, then there was a very slight peak shift for the (001) plane of ZrB_2 at ~25.2^{o}. The peak for the sintered ceramic moved very slightly towards a lower angle and approached the values given in the relevant JCPDF card (34-

0432), Figure 5b. Increasing the sintering temperature to 2000°C resulted in no further changes on the relative intensity or position of the peaks. Since there was no peak shift for the *h*BN peak in Figure 5b, instrumental error can be ruled out for the movement of the ZrB_2 peak. Therefore, the higher 2θ value for the as-synthesised powder is probably due to a slight decrease in the lattice parameter of the ZrB_2, which might result from residual nitrogen atoms in the ZrB_2 lattice. If true and the evidence is admittedly slim, then this phenomenon is inconsistent with previous phase equilibria studies on the ZrN-ZrB_2 pseudo-binary system at 1100°C [21]. After a 20 min hold, all the ZrB_2 peaks returned to the position indicated on the JCPDF card (34-0432), implying that most of the dissolved nitrogen atoms had come out of the ZrB_2 crystal structure.

Typical *h*BN flakes with different thickness were found in the ZBN composite sintered at different temperatures from 1100°C to 2000°C (Fig.3 d& e and Fig.4c& d). Nevertheless, only the pulling out of very thin hBN layers (<100nm) were observed on their fracture surface (Fig.3c&f). The thin hBN flake seems irrelevant with the sintering temperature and even the original thickness of hBN grains in the sintered body (Fig.3d&e). The local microstructure of the ZBN composite sintered at 2000°C was examined by TEM (Fig 6a), the presence of amorphous impurities are indicated by the arrow in Figure 6b, which was taken at a higher magnification. Near the impurities, microcracking normally existing in the BN flakes could be clearly recognized (6b, f and g). An amorphous Mg-Ca-Al-O-K (confirmed by EDS in Fig.6c) phase shows a poor wetting ability with the nearby ZrB_2/hBN grain boundaries, as the adjacent ZrB_2/hBN grain boundary looks very tight and clean, regardless of whether the basal (6e), or prism plane (6d), of the *h*BN is in contact with the ZrB_2 grains.

*h*BN has a strongly anisotropic thermal expansion. The thermal expansion coefficient (TEC) value for the c-axis of *h*BN has been measured as (38 – 40)×10^{-6} K^{-1}, which is approximately 40 times higher than that for its a-axis, (-2.7) – (-2.9)×10^{-6} K^{-1} [22]. In spite of the fact that a TEC difference does exist in ZrB_2 with its hexagonal symmetry, the difference between the c and a-axes of ZrB_2 is negligible if the number was compared with *h*BN. Assuming the thermal expansion of ZrB_2 is isotropic and the averaged TEC is 6.8×10^{-6} K^{-1}[2], the TEC mismatch between hBN and ZrB_2 will create residual stress in ZBN body during cooling inevitably. Interestingly, given the magnitude of the difference in the *h*BN, the direction of the residual stress will differ in the ZrB_2 grain, depending on which *h*BN plane faced towards

it. For instance, as marked in Fig.6i, tensile stress is available in ZrB_2 (I) and (III), because the TEC of *h*BN in c-axis is much larger than that in ZrB_2; in another grain, ZrB_2 (II), since the TEC of *h*BN in a-axis is much smaller than that in ZrB_2, the residual stress near the grain boundary must be compressive.

Now, given the cleanliness of the grain boundaries between the ZrB_2 and *h*BN grains as observed from the HRTEM images, Figure 6d and e, it is likely that the bonding between them will be strong. If it is assumed that the interfacial strength between the ZrB_2 and *h*BN is larger than the layer bonding strength in *h*BN then a sufficiently high tensile residual stress across the c-axis in the *h*BN grains could result in the latter being cleaved between their layers, as apparently seen in Figures 6f and h. Of course, a compressive stress is acting on the a-axis of the same *h*BN grain, so the synergetic effects of these two factors might induce a bridging structure between the delaminated *h*BN layers, as marked in Figure 6g. Based on the above discussion, the cleavage and pulling out of thin hBN layers in Fig.3c and f just mirrors the spontaneous microcracking phenomena in hBN grains, as revealed by the detailed TEM analysis.

Along with the increased relative density, the ZrB_2 grain size also becomes larger and its distribution becomes wider at a higher sintering temperature (Fig.7). The BN grains, which developed a lamellar shape, are homogenously distributed in the ZrB_2 matrix at all the sintering temperatures (Fig.3 and 4). Large voids were found in the pellet just after SHS (arrowed in Fig.3a), which disappeared after holding at 1100 ^{o}C. In line with this, compaction by removing the voids and rearranging the fine powders constitutes the main densification mechanism of ZBN composite which works at 1100^{o}C, though the formation of initial necking between adjacent ZrB_2 grains and its grain coarsening (from 200nm to 500nm, Fig.7) also could be found at this temperature (Fig.3d).

Apparently, curved boundary i.e. ZrB_2/BN or ZrB_2/ZrB_2 is the predominant feature in ZBN composite densified below 1700 ^{o}C, while most of the grain boundaries were developed into straight line with edges in the sample sintered at 2000 ^{o}C (Fig.4d and 6a). As we know, activated grain boundary will migrate towards the curvature in order to minimize the system energy, consequently, the rapid ZrB_2 grain growth between 1700 and 2000^{o}C (1.5μm

to 3μm, Fig.7) should be stemmed from the faster motion of Zr or B atom across ZrB_2/ZrB_2 and ZrB_2/BN grain boundary during this temperature range.

3.3 Mechanical properties

The mechanical properties of ZBN composites sintered at different temperatures are listed in Table I. As expected, at room temperature, the hardness of ZBN varied from 5.9 to 6.7 GPa, which is approximately equal to one third of the 18 – 20 GPa of ZrB_2 ceramics [2]. The incorporation of a large fraction of the softer *h*BN phase will have led to this significant decrease. In terms of increasing sintering temperature, the hardness value initially increased due to the increase in density but reached a peak at the sintering temperature of 1700^{o}C. According to the Hall-Petch equation, the decrease at 2000^{o}C might be related to the larger grain size in the sample exceeding the effect of the increasing density.

Changing sintering temperature from 1100^{o}C to 2000^{o}C, the room temperature Young's modulus (E) of ZBN composite increased steadily, i.e. from 183.5 GPa at 1100^{o}C to 206.4 GPa at 2000^{o}C. The results are reasonable since about 6% and nearly no porosity existed in the sample densified at 1100^{o}C and 2000^{o}C, respectively. Assuming a Young's modulus of 489 GPa for dense ZrB_2 and 80GPa for *h*BN ceramics, the upper bound, E_U ($E_U=\sum E_iV_i$, i stands for the component phase i and V_i is the volume percent for phase i, similarly hereinafter) and lower bound, E_L ($E_L^{-1}=\sum E_i^{-1}V_i$) for ZBN ceramics were calculated to be 337.7GPa and 166.8GPa, respectively. Evidently, all the measured values are located in the gap between E_U and E_L. In contrast, the poisson's ratio changed very little with sintering temperature and all of the values were only slightly higher at 0.15-0.16 than the reported value of 0.14 for monolithic ZrB_2. This suggests that the variation in density, grain size and, indeed, composition were all too small to have a substantial effect. The sintering temperature dependence of shear modulus (G) of ZBN composites followed a similar trend to the elastic modulus, due to the similar level of poisson's ratio in these samples and the inherent relationship among the elastic constants.

The critical *h*BN volume (V_c) required to form a percolated microstructure in ZrB_2-BN ceramics can be calculated based on Eq.1. The particle packing parameter here is set as 1.27, which has been verified to have little influence on the calculation of V_c [23].

$$V_c = \frac{100}{1 + 0.32 / X_c (R_z / R_B)} \qquad \text{(Eq.1)}$$

From our previous work it is known that after reaction 1 has completed, a very thin layer of *h*BN is homogenously coated on the surface of the ZrB_2 particles so X_c is equal to 1 in this case and R_Z/R_B should be much larger than 10. Therefore, as calculated, V_c should be smaller than 23 vol%. The upper bound of calculated V_c is similar to the percolation threshold recognized for a randomly distributed two-phase system, which is ~20 vol% [24]. Taking into account that, at 37 vol%, the volume fraction of *h*BN in the ZBN composite is above this value, the formation of an interconnected three-dimensional *h*BN network in ZBN is likely, based on the percolation theory.

The room temperature bending strengths of the as-sintered ZBN composites were relatively low, which can be attributed to both the levels of residual porosity in the samples sintered at less than 1700°C and the presence of the low Young's modulus *h*BN phase located throughout the ZrB_2 matrix. The *h*BN grains were observed to be interconnected in all of the samples, no matter what sintering temperature was employed, Figures 3 and 4. The presence of such continuous channels of weak *h*BN might assist crack propagation before fracture. The measured values for the ZBN composites ranged from about 200 to about 350 MPa, Table I, again with a maximum for the sample sintered at 1700°C suggesting that density was again the primary factor at lower temperatures and porosity and grain size affected the sample sintered at 2000°C as for the hardness.

Although only limited high temperature bending strength tests were conducted at 1300°C on selected ZBN composites, the trend was essentially the same as for the room temperature strengths but the values were all approximately halved, ranging from about 100 to 200 MPa. A representative load/displacement plot for the ZBN composite sintered at 2000°C is shown in Figure 8a. At room temperature, the plot shows classic brittle behaviour until failure, however there was more plastic deformation when the samples were tested at 1300°C, indicating the bars suffering creep damage. From the TEM observation discussed

earlier, residual amounts of amorphous phases composed of Mg-Ca-Al-O-K were observed in the ZrB_2-*h*BN-*h*BN triangular grain boundaries, Figure 6b and evidence for this impurity phase softening was also detected in the composite's microstructure, see the arrows in Figure 8b. Although the macroscopic creep of ZrB_2-based ceramics and their corresponding decrease in strength at around 1300^{o}C has been assigned to the softening of oxide impurities at the triple junctions [25], for the ZBN composite, this should be attributed to the softening of the amorphous Mg-Ca-Al-O-K phase. The precursor boron powder is one potential source which is able to provide and trap the impurities in terms of Mg, K etc. into ZBN composite. Accordingly, in the future work, a new, higher purity, submicron boron powder will be used with a view to improving the elevated temperature mechanical properties of ZBN composites.

3.4 On the possibility of implementing reactively densified ZBN composite as the matrix for long SiC fiber-based composites

3.4.1 Chemical compatibility of SiC_w in ZrN-B mixture

Although no work on the possibility of using ZBN as a matrix for SiC fibre-based composites has been done to date, it is perhaps worth speculating on the potential for the matrix based on the known results to date. Both of ZrB_2 and *h*BN are characterized as difficult-to-densify ceramics. Reported sintering temperatures varied for ZrB_2-*h*BN composites, but most of them are located between 1800^{o}C and 2200^{o}C either by SPS or hot pressing, in order to reach a relative density above 90%. Giving consideration to the ultra-low sintering temperature (1100^{o}C) for reaching a similar level of density in this work, the degradation of SiC_f in the post processing could be avoided if ZrB_2-BN composites developed here were used as its matrix. However, there is still the possibility that chemical reactions could occur between the SiC, B and ZrN prior to or during the boronizing of the ZrN. For this purpose, β-SiC whisker was used as an analogue to simulate the behavior of SiC_f in ZrN-B mixture during heating. The sintering of ZBN with 10wt% SiC_w composites was undertaken at 1550^{o}C, which is well above the peak recorded temperature for the exothermic reaction seen in Figure 1. The polished surface of sintered ZrB_2-BN-SiC_w was shown in Fig. 9.

Most of SiC_w kept their original morphology, no obvious reactions and byproducts were observed between the whiskers and ZrB_2-BN matrix, although there was some evidence of surface roughness and breakage of the whiskers, highlighted by arrows in Figure 9. Together with the reaction 1 and a pressure of 60MPa, a huge shrinkage was generated on the starting powder mixture during heating. Just formed ZrB_2-BN nano powders are capable to consume such deformation in terms of grain sliding or even densification. Nevertheless, rearranging these randomly distributed SiC_w with large aspect ratio under pressure is more difficult, which might be responsible for the formation of microcracking and other defects in SiC_w (arrowed in Fig.9). More careful work on decreasing the levels and the applying speeds of the load seems to be useful to address this issue according to our ongoing work.

3.4.2 The possibility for pulling out of SiC fiber during fracturing

Based on the porosity left in composites, the references associated with on long fiber reinforced UHTCs could be mainly classified into two categories:

(i) The matrix is constituted by dense ceramics, i.e. C_f or SiC_f/ZrB_2-$ZrSi_2$ (matrix) [5, 7] and C_f or SiC_f /BN (intermediate layer)/ ZrB_2-$ZrSi_2$ (matrix) [26];

(ii) Porous matrix materials, mainly includes non-sintered UHTC particles connected by pyrolytic carbon [11].

The E moduli of SiC fiber (400GPa) and high strength Carbon fiber (200-300GPa) are smaller than dense UHTCs (480-500GPa), even an external *h*BN was coated on the fiber. In type i, under a fixed level of tensile stress, the strain of the fiber must be larger than that of the matrix, resulting from its lower modulus. Consequently, fiber has to bear all the loadings at this stage. If fiber fails to do so, failure will initiate from the defects in the fiber. With further increasing the loads, ceramic matrix constitutes the failure of the composite, indicating the composite will show a brittle fracture in the end and the pulling out of fiber should be rare [27].

In Type ii, on the contrary, matrix breaks in prior to the fiber originating from its lower modulus in porous body (matrix). The fiber should be able to retain the broken matrix in place until it breaks at its terminal load. In this case, continuous fiber breakage and its pulling out should be observed. The problem resting in Type II is that the current developed matrix is mainly formed by loosely packed powders which are not sintered. Hence, nearly no

contribution on the total strength of the composites has been made by the matrix, the strength is highly relied on the quality, fraction and weaving of the fiber preform.

Herein, low temperature reactively densified ZrB_2-BN ceramics are proposed for using as a new matrix for CF-UHTCs. In view that as measured modulus of ZBN composite (180-200 GPa) is much lower than the corresponding value of SiC and carbon fiber, the new composite should be classified into Type II. In spite of this, the new SiC_f (C_f)/ZrB_2-BN composites should show totally different fracture behaviors from the current porous matrix being used. The reason is that ZrB_2-BN ceramics in dense nature will afford and share the stress before its breakage. Specimens should still exhibit a non-catastrophic failure as discussed above, as a result of the pulling out of the fiber following. Moreover, *h*BN in ZBN matrix could protect the SiC_f through avoiding the reaction between oxide impurities and SiC_f. At last, the spontaneous microcracking of *h*BN in ZBN, as verified in 3.2, is also helpful for realizing the pull-out of the fiber, due to the week bonding available between reinforced element and SiC fiber.

4. Conclusion

Densification of hard-to-densify ZrB_2-BN ceramics (ZBN) was realized at temperatures lower than 1550^{o}C by a reactive approach from inorganic precursors, i.e. ZrN and boron. A huge shrinkage took place together with the reaction during heating. Sample with ZrB_2 average grain size of ~500nm could be sintered to 94% of its theoretical densify after holding at 1100^{o}C for 20min, under a pressure of 60MPa. With further elevating the sintering temperature to 1550 and 1700^{o}C, the grain size of ZrB_2 gradually increased to 1.5 and 1.7μm in a dense ceramic body. No further phase change was observed on the sample densified 2000^{o}C, but the rapid ZrB_2 grain growth occurred and its distribution also became wider. Percolated microstructure was found on the ZrB_2-BN ceramics sintered from 1100-2000^{o}C, due to the volume of hBN exceeds the critical value calculated from the percolate theory. Resulting from the interconnected weak phase of BN, relatively low hardness, strength and Young's modulus were measured in ZBN composite, which varied slightly with the sintering temperatures. Microcracking in *h*BN was detected from TEM analysis together with the accumulation of a small amount of low melting point impurities at the triple junctions,

yielding the formation of an amorphous phase of Mg-Ca-Al-O-K and is responsible for the strength degradation of ZBN composite at 1300^{o}C.

Sintered ZBN composite shows a much lower modulus (180-200GPa) compared to the SiC fiber (400GPa). This feature differentiates ZrB_2-*h*BN from the other dense UHTC matrix being used and it would facilitate the fiber pulling out process. Furthermore, no visible reactions between SiC_f and ZrN-B were found on sintered ZrB_2-*h*BN-SiC_w from powder mixture contains SiC_w, ZrN and B. Owing to these two merits, employing ZBN as the matrix for long fiber reinforced ceramics is fairly feasible.

Acknowledgements

The work was jointly supported financially by a grant from the NSFC (No. 51272266) from the Chinese government and the Swedish Research Council on Ceramics With Deeper Structural Heterogeneities. Dr Ji Zou was supported by an EPSRC grant entitled Material Systems for Extreme Environments, XMat (EP/K008749/2). Parts of this work were done by Ji Zou when he was an exchange student in KU Leuven in 2009, which was funded by the research fund of K.U. Leuven in the framework of the Flanders-China bilateral project BIL 07/06.

References

[1] F. Monteverde, R. Savino, Stability of ultra-high-temperature ZrB_2–SiC ceramics under simulated atmospheric re-entry conditions, ***J. Euro. Ceram. Soc***. 27(2007) 4797-4805.

[2] W. G. Fahrenholt and G. E. Hilmas, Refractory diborides of zirconium and hafnium, ***J. Am. Ceram. Soc***. 90(2007) 1347-64.

[3] E. Wuchina, E. Opila, M. Opeka, W. Fahrenholtz, and I. Talmy, UHTCs: Ultra-High Temperature Ceramic Materials for Extreme Environment Applications, ***The Electrochemical Society Interface, Winter***, 16(2007)30–36.

[4] J. Zou, G. J. Zhang and Y. M. Kan. "Formation of tough interlocking microstructure in ZrB_2-SiC based ultra high temperature ceramics by pressureless sintering" ***J. Mater. Res***., 24(2009) 2428-34.

[5] L. Zoli, V. Medri, C. Melandri and D. Sciti, Continuous SiC fibers-ZrB_2 composites, ***J. Euro. Ceram. Soc.*** 35(2015)4371-76.

[6] R. Bodet, X. Bourrat, J. Lamon, and R. Naslain, Tensile Creep Behaviour of a Silicon Carbide-Based Fibre with a Low Oxygen Content, ***J. Mater. Sci***., 30(1995) 661–77.

[7] Laura Silvestroni, Daniele Dalle Fabbriche, Diletta Sciti, Tyranno SA3 fiber-ZrB_2 composites. Part I: Microstructure and densification. ***Materials and Design*** 65 (2015) 1253–1263.

[8] T. Ishikawa, Y. Kohtoku, K. Kumagawa, T. Yamamura, and T. Nagasawa, High-Strength Alkali-Resistant Sintered SiC Fibre Stable to 2200°C, ***Nature***, 391(1998) 773–75.

[9] Yonggang Tong, Shuxin Bai, Ke Chen, C/C-ZrC composite prepared by chemical vapor infiltration combined with alloyed reactive melt infiltration. ***Ceram. Inter.*** 38 (2012) 5723–5730.

[10] D. D. Jayaseelan, R. G. de Sá, Peter Brown and William E. Lee, Reactive infiltration processing (RIP) of ultra high temperature ceramics (UHTC) into porous C/C composite tubes, ***J. Euro. Ceram. Soc.*** 31 (2011) 361–368.

[11] A. Paul, S. Venugopal, J.G.P. Binner, B. Vaidhyanathan, A.C.J. Heaton, P.M. Brown, UHTC–carbon fibre composites: Preparation, oxyacetylene torch testing and characterisation, ***J. Euro. Ceram. Soc.*** 33 (2013) 423–432.

[12] Z.J. Dong, S.X. Liu, X.K. Li, A. Westwood, G.M. Yuan, Z.W. Cui and Y. Cong, Influence of infiltration temperature on the microstructure and oxidation behavior of SiC–ZrC ceramic coating on C/C composites prepared by reactive melt infiltration. ***Ceram. Inter.*** 41 (2015) 797–811.

[13] K. Park and T. Vasilos, Processing, Microstructure and Mechanical Properties of Hot Pressed SiC Continuous Fibre/SiC Composites, ***J. Mater. Sci.*** 32(1997) 295–300.

[14] Shaoming Dong, Yutai Katoh, and Akira Kohyama, Preparation of SiC/SiC Composites by Hot Pressing, Using Tyranno-SA Fiber as Reinforcement, ***J. Am. Ceram. Soc***. 86(2003) 26–32.

[15] S. C. Zhang, G. E. Hilmas and W. G. Fahrenholtz, Pressureless Densification of Zirconium Diboride with Boron Carbide Additions, ***J. Am. Ceram. Soc.*** 89(2006) 1544-50.

[16] L. Silvestroni, H.J. Kleebe, S. Lauterbach, M. Müller and D. Sciti, Transmission electron microscopy on Zr- and Hf-borides with $MoSi_2$ addition: Densification mechanisms, ***J. Mater. Res***. 25(2010) 828-34.

[17] S. Q. Guo, Y. Kagawa and T. Nishimura, Mechanical behavior of two-step hot-pressed ZrB_2-based composites with $ZrSi_2$, ***J. Euro. Ceram. Soc.*** 29 (2009) 787–794.

[18] Ji Zou, Jingjing Liu, Guo-Jun Zhang, Shuigen Huang, Jef Vleugels, Omer Van der Biest and James Zhijian Shen, Hexagonal BN-encapsulated ZrB_2 particle by nitride boronizing. ***Acta Materialia*** 72 (2014) 167–177

[19] Vanmeensel, K, Laptev, A, Hennicke, J Vleugels and Van der Biest, O. (2005). Modelling of the temperature distribution during field assisted sintering. ***Acta Mater.*** 53(2005) 4379-4388.

[20] Witold Brostow, Brian P. Gorman, Oscar Olea-Mejia, Focused ion beam milling and scanning electron microscopy characterization of polymer +metal hybrids, ***Materials Letters*** 61 (2007) 1333–1336.

[21] E. Rudy and F. Benesovsky, Investigations in the systems: hafnium-boron-nitrogen and zirconium-boron-nitrogen (in Germany), Monatsh. Chem., 92(1961) 415-441.

[22] W. Paszkowic, J.B. Pelka, M. Knapp, T. Szyszko and S. Podsiadlo. Lattice parameters and anisotropic thermal expansion of hexagonal boron nitride in the 10–297.5 K temperature range. ***Applied Physics A*** 75(2002) 431-435.

[23] R. P. Kusy, Influence of Particle Size Ratio on the Continuity of Aggregates, ***J. Appl. Phys***. 48(1977) 5301-5.

[24] Guo-Jun Zhang and Tatsuki Ohji, Effect of BN content on elastic modulus and bending strength of SiC–BN in situ composites. ***J. Mater. Res***. 15(2000) 1876-80.

[25] J. Zou, G. J. Zhang, C. F. Hu, T. Nishimura, Y. Sakka, H. Tanaka, J. Vleugels and O. Van der Biest. High-temperature bending strength, internal friction and stiffness of ZrB2-20vol%SiC ceramics. ***J. Euro. Ceram. Soc.*** 32(2012) 2519-2527.

[26] Laura Silvestroni, Diletta Sciti, Greg E. Hilmas, William G. Fahrenholtz and Jeremy Watts, Effect of a weak fiber interface coating in ZrB2 reinforced with long SiC fibers, ***Materials and Design*** 88 (2015) 610–618.

[27] Laura Silvestroni, Diletta Sciti, Cesare Melandri, Stefano Guicciardi, Tyranno SA3 fiber–ZrB_2 composites. Part II: Mechanical properties. ***Materials and Design*** 65 (2015) 1264–1273.

Figure captions

Fig.1 Temperature, loading profile and punch displacement observed during SPS sintering of ZBN composites sintered at a) 1100^{o}C and b) 1550^{o}C.

Fig.2 The effects of temperatures and holding time on the relative density and open porosity of ZBN composites.

Fig.3 Fracture surfaces of ZBN composites: (a) Just after the exothermic reaction; (b) after holding at 1100^{o}C for 20 min, low magnification; (c) after holding at 1100^{o}C for 20 min, high magnification; (f) after holding at 1550^{o}C for 20min. (d) and (e) show the polished surfaces of ZBN composites sintered at 1100^{o}C and 1550^{o}C, respectively. The polishing was achieved using a FIB.

Fig.4 4 (a) and (b) show the fracture surfaces of ZBN composites sintered at 1700^{o}C and 2000^{o}C for 20 mins, respectively, whilst their polished surfaces are shown in (c) and (d), note the differences on the scale bars in these images.

Fig.5 (a) The XRD patterns of ZBN composites sintered at different temperatures, whilst (b) reveals that a noticeable peak shift for the ZrB_2 phase occurred in the samples just after Reaction 1.

Fig.6 TEM analysis of a ZBN composite sintered at 2000^{o}C: (a) low magnification; (b) with impurities arrowed and obvious microcracking in the *h*BN; (c) the EDS pattern of the arrowed phase in b; (d) and (e) are the HRTEM images showing clean grain boundaries between ZrB_2 and two typical *h*BN planes, (d) prism plane and (e) basal plane; the detailed microcracking in *h*BN is displayed in (g) and (f), with corresponding electron pattern shown in (h). The as-indexed zone axis in (h) is [100], therefore, the layered atomic plan in *h*BN (6f and 6g) is its basal plane. The direction of the different residual stresses on the *h*BN grain in (f) is depicted in (i).

Fig.7 The ZrB_2 grain size distribution in ZBN composites as a function of sintering temperature.

Fig.8 The load-displacement curve for ZBN composites specimens tested at room temperature (RT) and 1300^{o}C; (b) shows the resulting fracture surface after the test undertaken at 1300^{o}C

Fig.9 The polished surface of ZBN-10wt %SiC_w, which was sintered at 1550^{o}C for 7mins.

Table caption

Table I Mechanical properties of ZBN composites sintered at different temperatures.

Table

Table I Mechanical properties of ZBN composites sintered at different temperatures.

Sintering temperature / ^{o}C	Hardness HV_1 / GPa	E modulus / GPa	G modulus / GPa	Poisson's ratio	Strength / MPa		Grain Size / ZrB_2
					RT	1300^{o}C	
1100	5.9±0.3	183.5±1.4	79.8±0.6	0.15	204±5	104±15	500 nm
1550	6.2±0.2	194.3±0.7	84.3±0.3	0.15	291±9	/	1.1 μm
1700	6.7±0.2	197.5±0.8	86.1±0.4	0.15	353±33	191±17	1.5 μm
2000	6.3±0.4	206.4±0.8	88.9±0.3	0.16	295±31	145±9	3.0 μm

Figure.1

Click here to download high resolution image

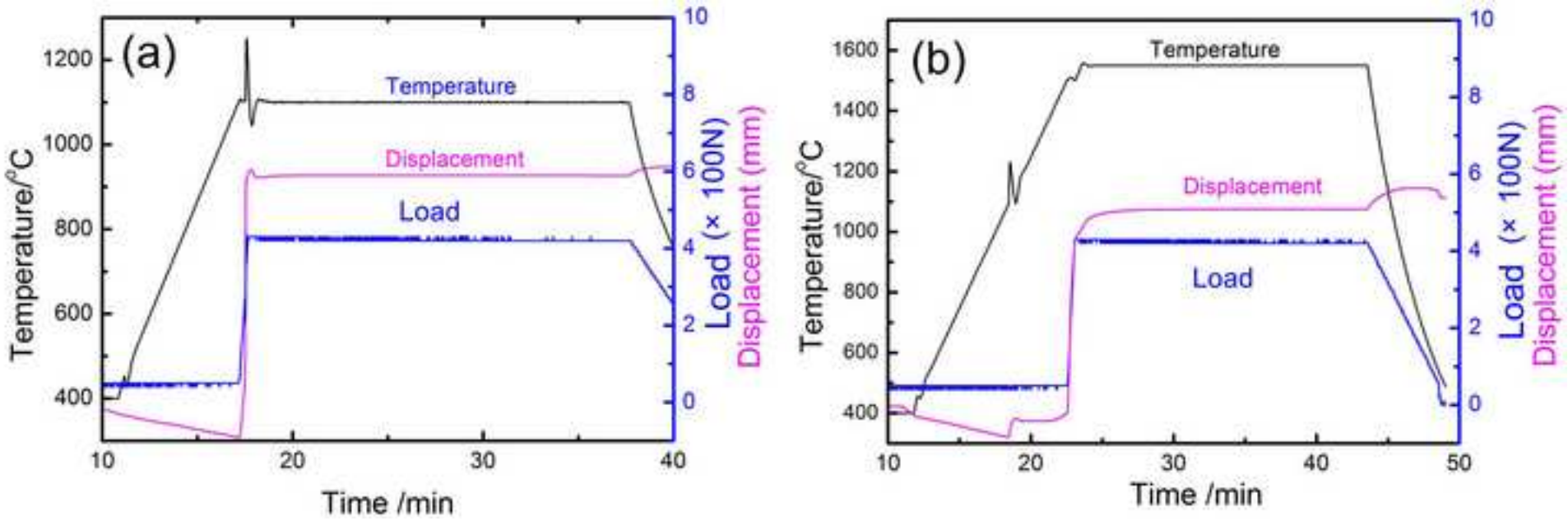

Figure.2
Click here to download high resolution image

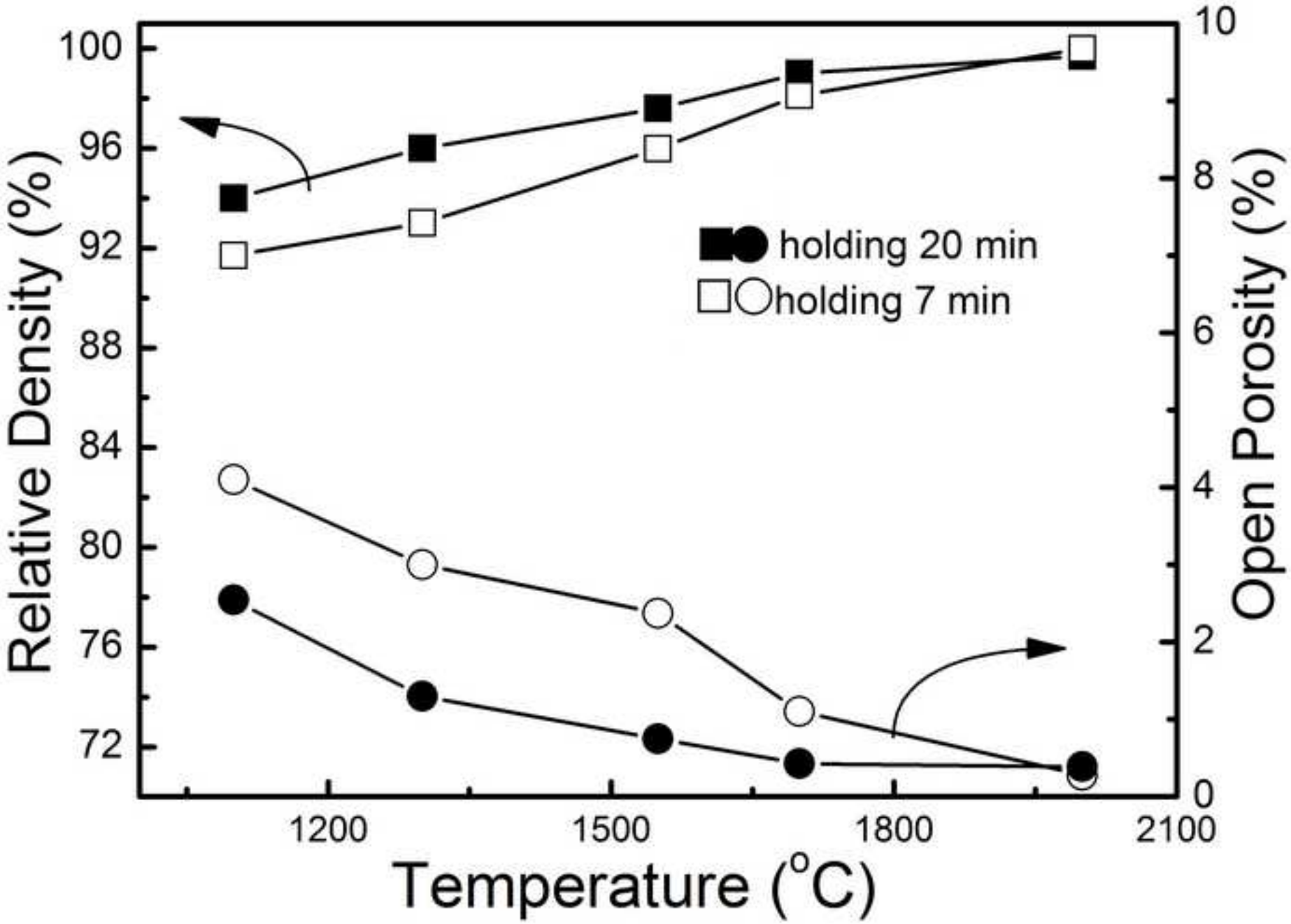

Figure.3
Click here to download high resolution image

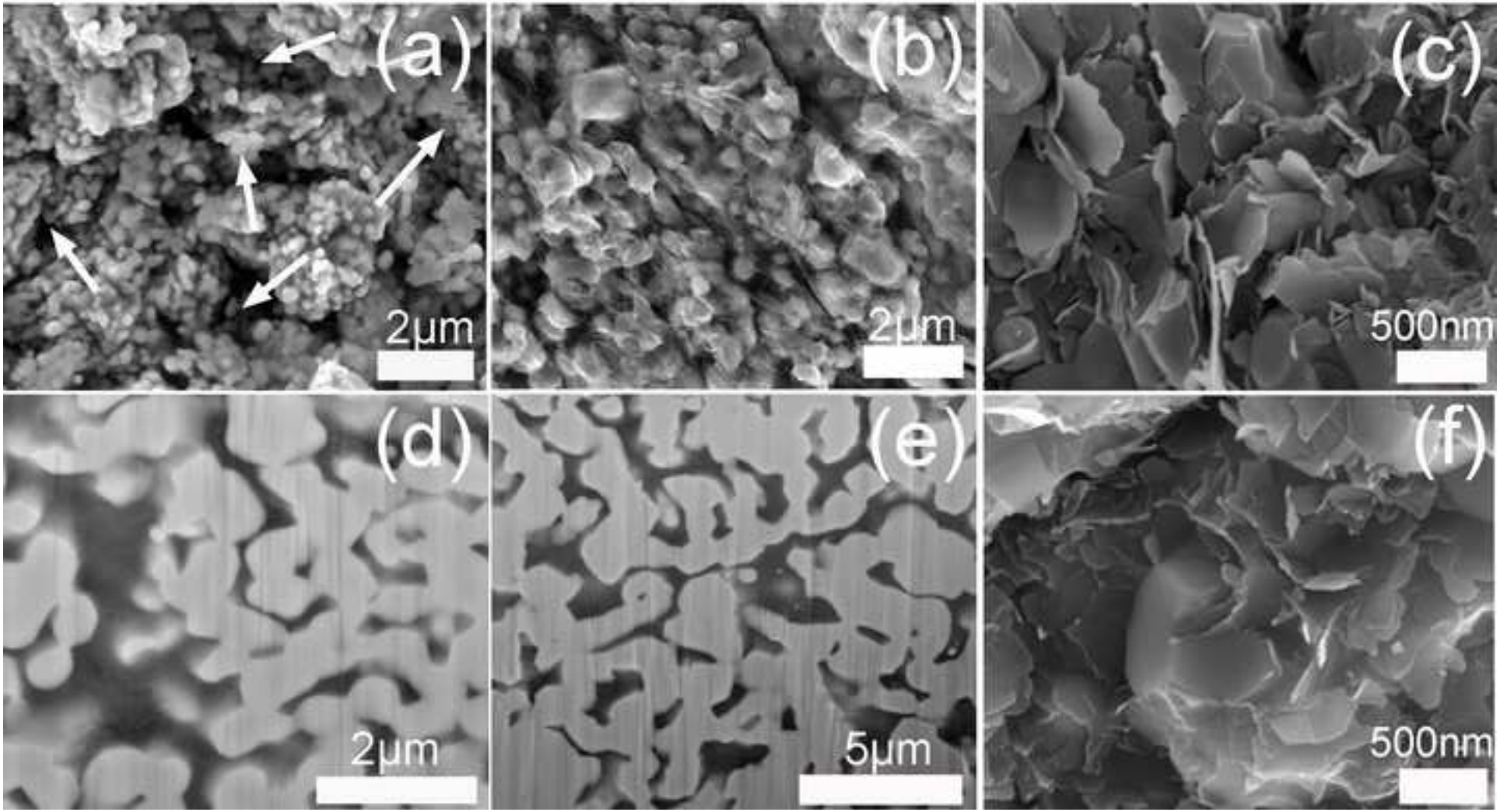

Figure.4
Click here to download high resolution image

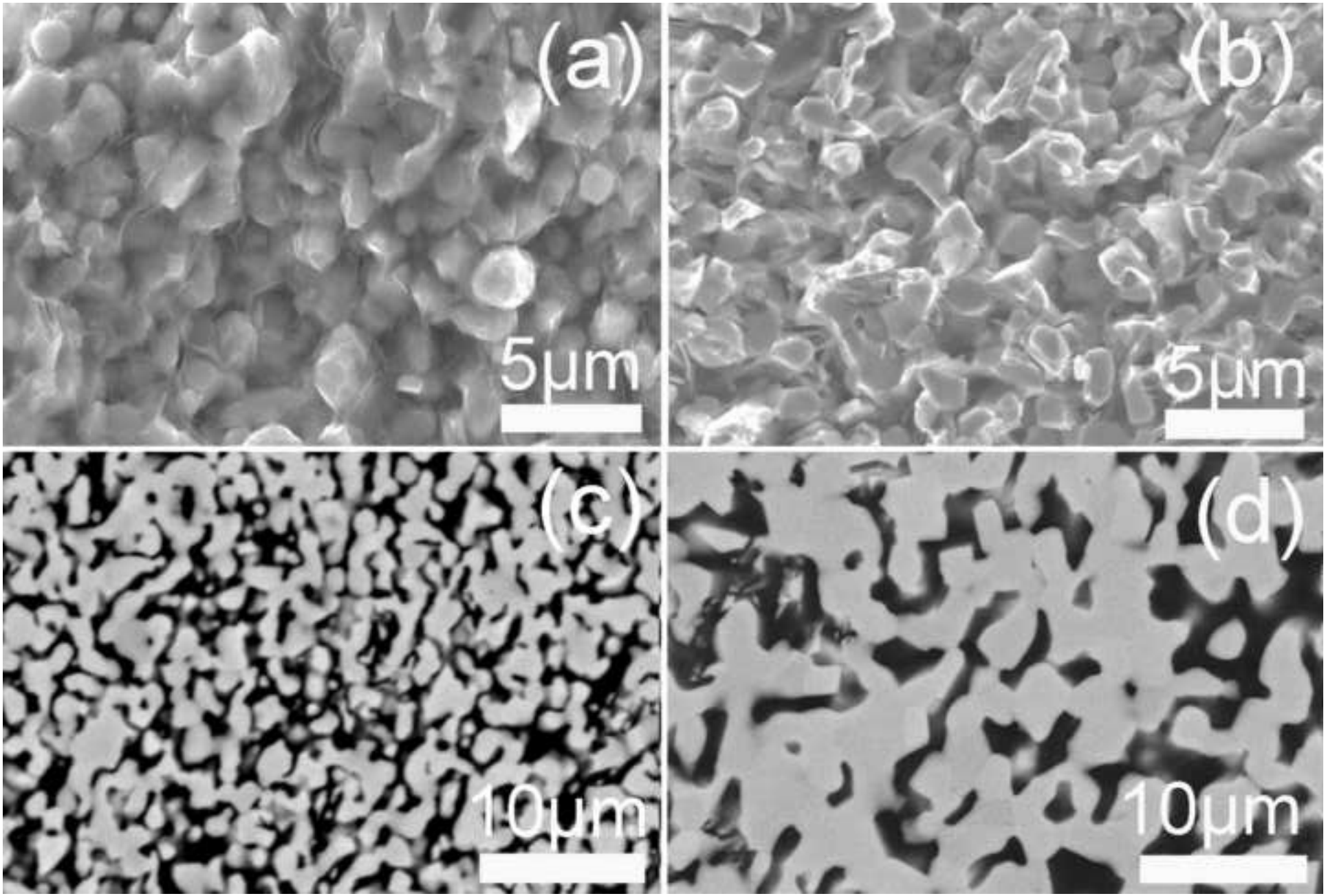

Figure.5

Click here to download high resolution image

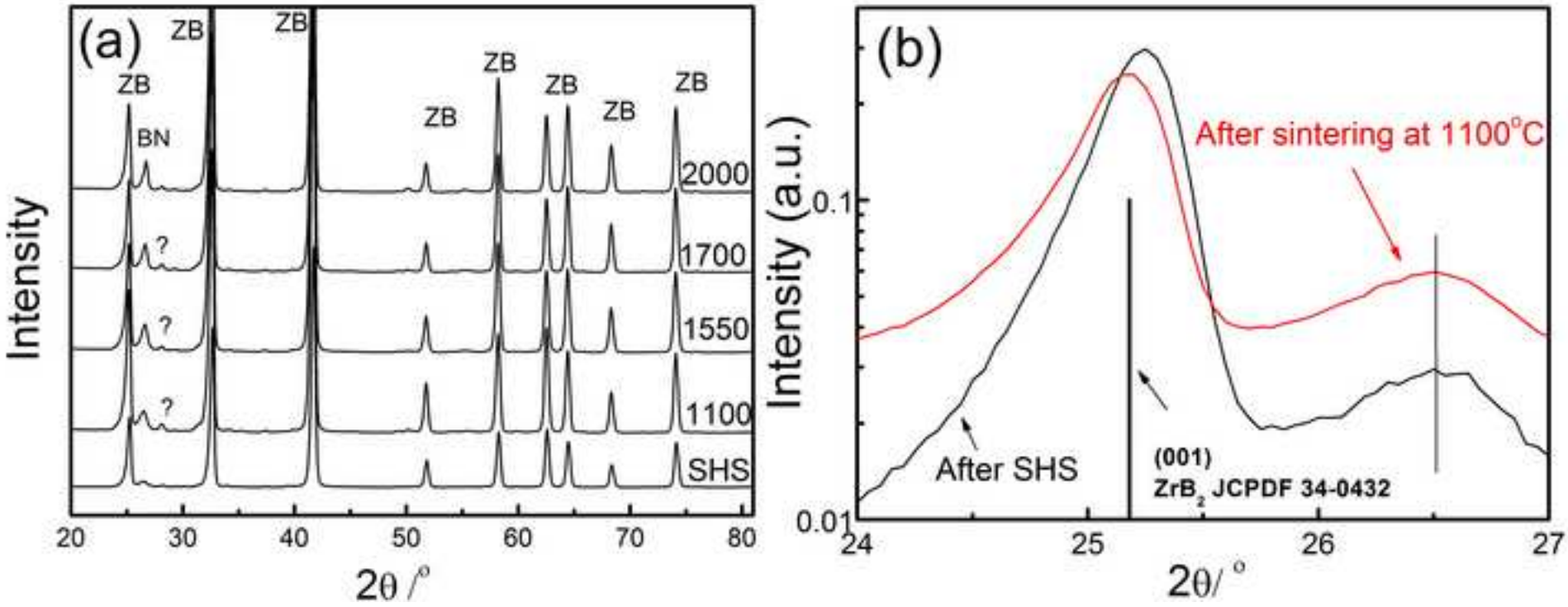

Figure.6

Click here to download high resolution image

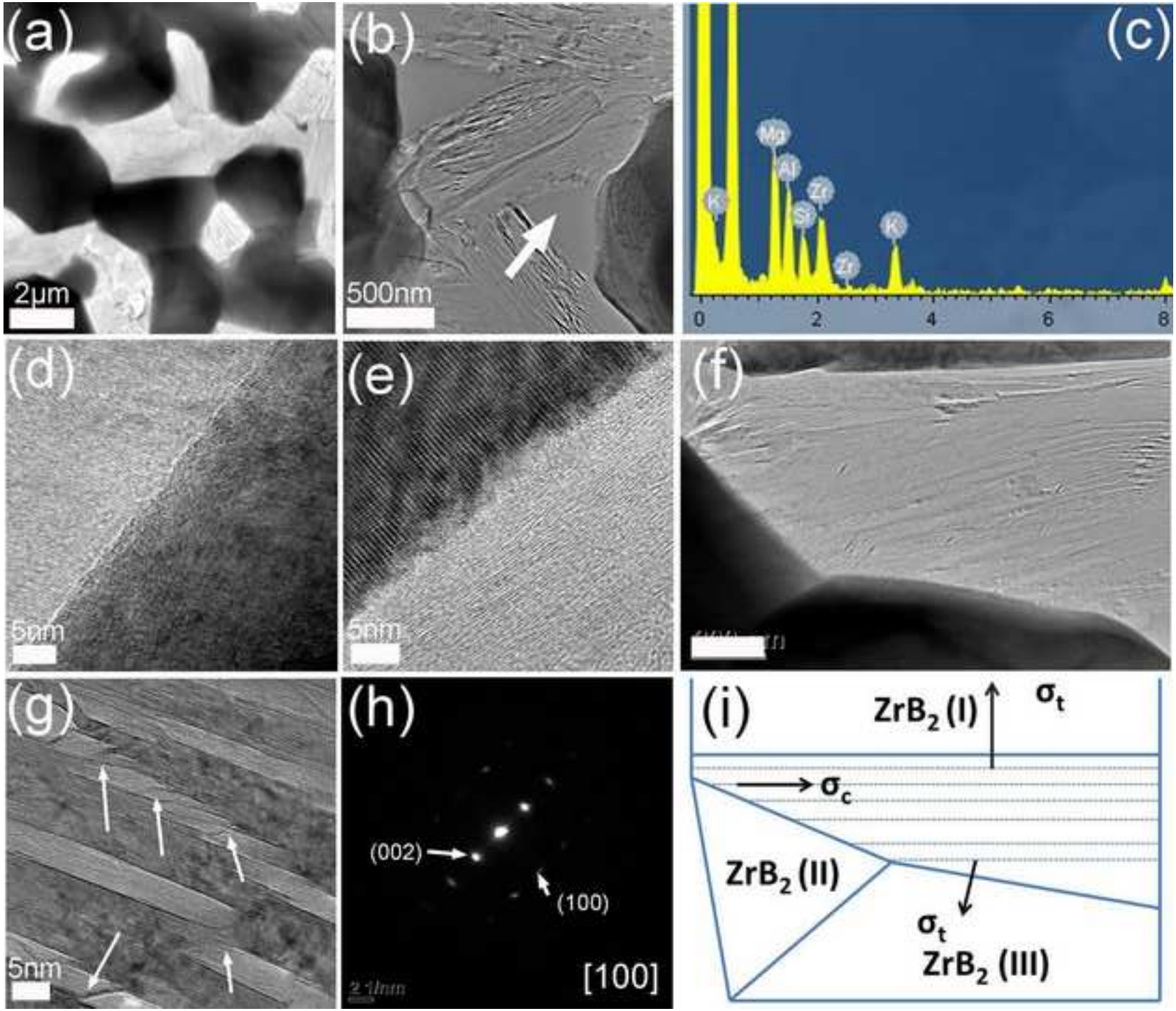

Figure.7

Click here to download high resolution image

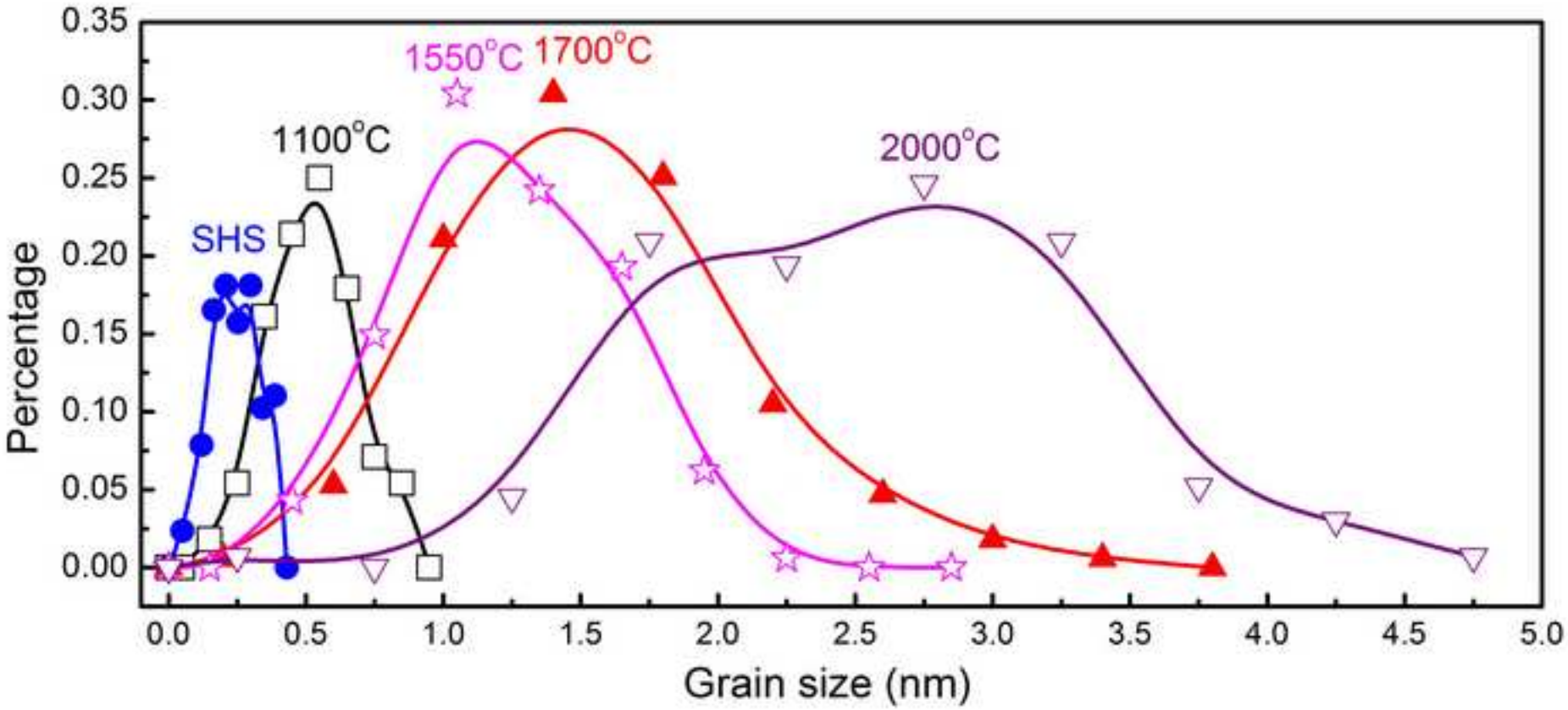

Figure.8
Click here to download high resolution image

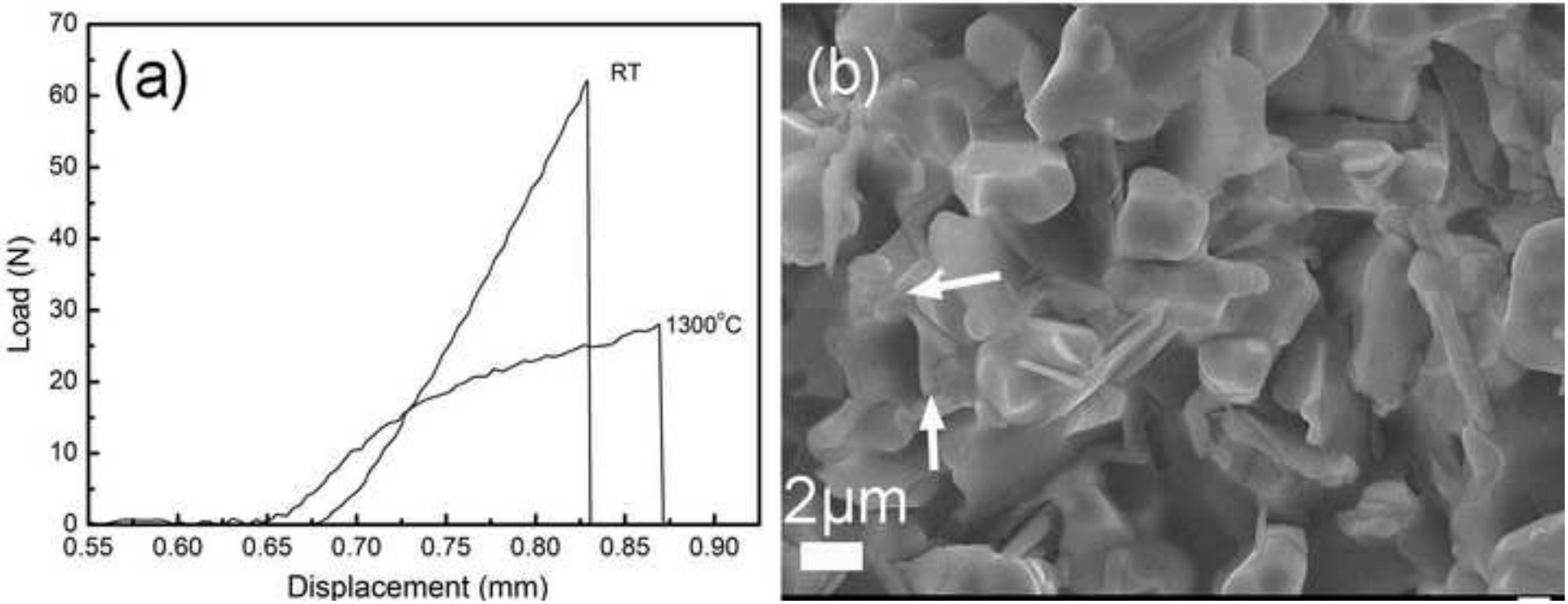

Figure.9

Click here to download high resolution image

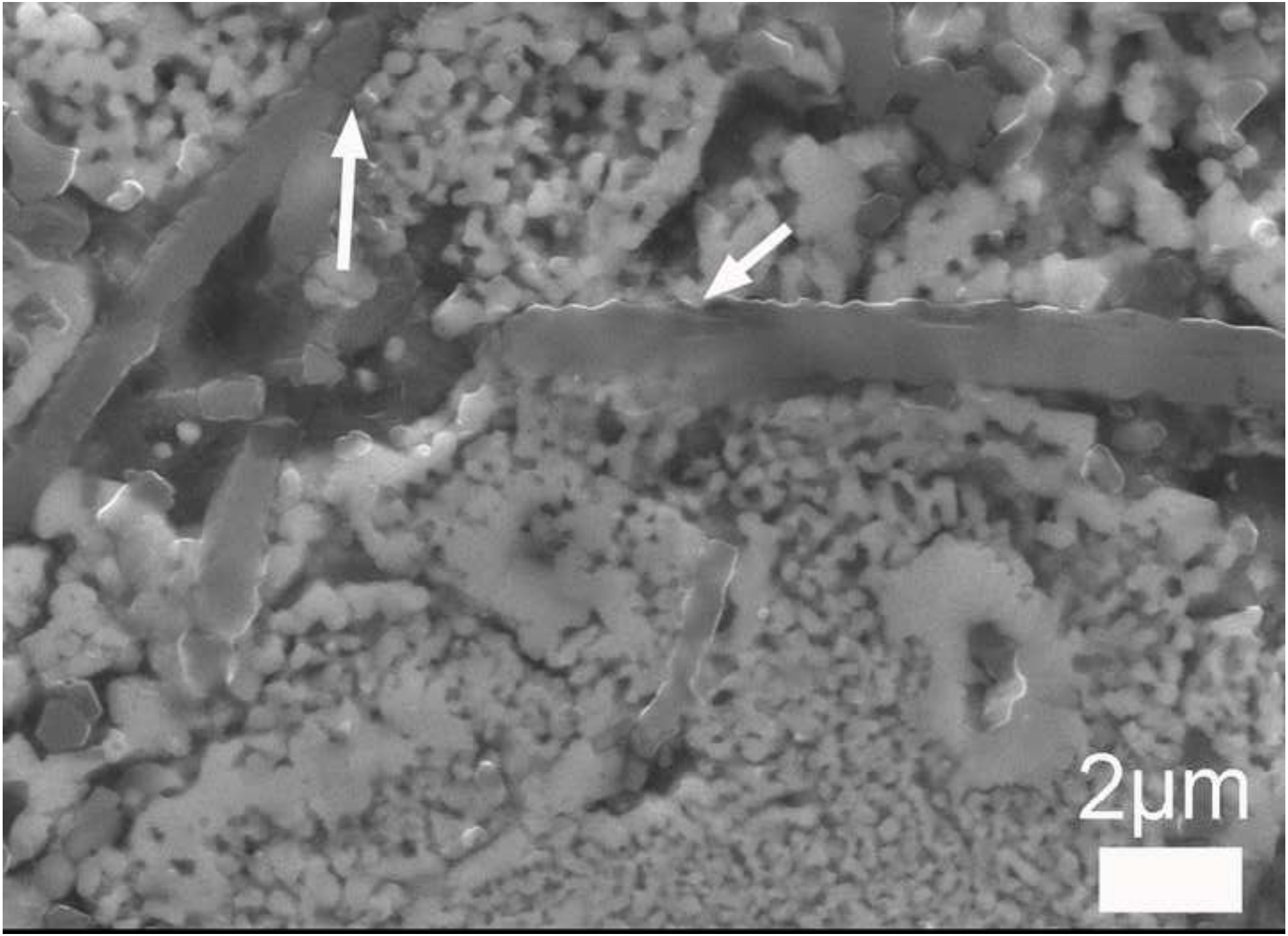

Figure captions

Fig.1 Temperature, loading profile and punch displacement observed during SPS sintering of ZBN composites sintered at a) 1100^{o}C and b) 1550^{o}C.

Fig.2 The effects of temperatures and holding time on the relative density and open porosity of ZBN composites.

Fig.3 Fracture surfaces of ZBN composites: (a) Just after the exothermic reaction; (b) after holding at 1100^{o}C for 20 min, low magnification; (c) after holding at 1100^{o}C for 20 min, high magnification; (f) after holding at 1550^{o}C for 20min. (d) and (e) show the polished surfaces of ZBN composites sintered at 1100^{o}C and 1550^{o}C, respectively. The polishing was achieved using a FIB.

Fig.4 4 (a) and (b) show the fracture surfaces of ZBN composites sintered at 1700^{o}C and 2000^{o}C for 20 mins, respectively, whilst their polished surfaces are shown in (c) and (d), note the differences on the scale bars in these images.

Fig.5 (a) The XRD patterns of ZBN composites sintered at different temperatures, whilst (b) reveals that a noticeable peak shift for the ZrB_2 phase occurred in the samples just after Reaction 1.

Fig.6 TEM analysis of a ZBN composite sintered at 2000^{o}C: (a) low magnification; (b) with impurities arrowed and obvious microcracking in the *h*BN; (c) the EDS pattern of the arrowed phase in b; (d) and (e) are the HRTEM images showing clean grain boundaries between ZrB_2 and two typical *h*BN planes, (d) prism plane and (e) basal plane; the detailed microcracking in *h*BN is displayed in (g) and (f), with corresponding electron pattern shown in (h). The as-indexed zone axis in (h) is [100], therefore, the layered atomic plan in *h*BN (6f and 6g) is its basal plane. The direction of the different residual stresses on the *h*BN grain in (f) is depicted in (i).

Fig.7 The ZrB_2 grain size distribution in ZBN composites as a function of sintering temperature.

Fig.8 The load-displacement curve for ZBN composites specimens tested at room temperature (RT) and 1300^{o}C; (b) shows the resulting fracture surface after the test undertaken at 1300^{o}C

Fig.9 The polished surface of ZBN-10wt %SiC_w, which was sintered at 1550^{o}C for 7mins.

Table caption

Table I Mechanical properties of ZBN composites sintered at different temperatures.